AD

TECHNICAL REPORT ARBRL-TR-02227

NUMERICAL SOLUTION OF THE AZIMUTHAL-INVARIANT THIN-LAYER NAVIER-STOKES EQUATIONS

Charles J. Nietubicz
Thomas H. Pulliam
Joseph L. Steger

March 1980

US ARMY ARMAMENT RESEARCH AND DEVELOPMENT COMMAND
BALLISTIC RESEARCH LABORATORY
ABERDEEN PROVING GROUND, MARYLAND

Destroy this report when it is no longer needed.
Do not return it to the originator.

Secondary distribution of this report by originating or sponsoring activity is prohibited.

Additional copies of this report may be obtained from the National Technical Information Service, U.S. Department of Commerce, Springfield, Virginia 22151.

The findings in this report are not to be construed as an official Department of the Army position, unless so designated by other authorized documents.

The use of trade names or manufacturers' names in this report does not constitute indorsement of any commercial product.

REPORT DOCUMENTATION PAGE

READ INSTRUCTIONS BEFORE COMPLETING FORM

1. REPORT NUMBER: TECHNICAL REPORT ARBRL-TR-02227
2. GOVT ACCESSION NO.:
3. RECIPIENT'S CATALOG NUMBER:

4. TITLE (and Subtitle): NUMERICAL SOLUTION OF THE AZIMUTHAL-INVARIANT THIN-LAYER NAVIER-STOKES EQUATIONS

5. TYPE OF REPORT & PERIOD COVERED: Final

6. PERFORMING ORG. REPORT NUMBER:

7. AUTHOR(s):
Charles J. Nietubicz
Thomas H. Pulliam
Joseph L. Steger

8. CONTRACT OR GRANT NUMBER(s):

9. PERFORMING ORGANIZATION NAME AND ADDRESS:
U.S. Army Ballistic Research Laboratory
(ATTN: DRDAR-BLL)
Aberdeen Proving Ground, Maryland 21005

10. PROGRAM ELEMENT, PROJECT, TASK AREA & WORK UNIT NUMBERS: RDT&E 1L161102AH43

11. CONTROLLING OFFICE NAME AND ADDRESS:
U.S. Army Armament Research & Development Command
U.S. Army Ballistic Research Laboratory
(ATTN: DRDAR-BL) Aberdeen Proving Ground, MD 21005

12. REPORT DATE: MARCH 1980

13. NUMBER OF PAGES: 37

14. MONITORING AGENCY NAME & ADDRESS (if different from Controlling Office):

15. SECURITY CLASS. (of this report): Unclassified

15a. DECLASSIFICATION/DOWNGRADING SCHEDULE:

16. DISTRIBUTION STATEMENT (of this Report):

Approved for public release, distribution unlimited.

17. DISTRIBUTION STATEMENT (of the abstract entered in Block 20, if different from Report):

18. SUPPLEMENTARY NOTES:

19. KEY WORDS (Continue on reverse side if necessary and identify by block number):
Finite Difference Techniques
Thin Layer Navier-Stokes Equations
Viscous Flow
Inviscid Flow
Hollow Projectile

20. ABSTRACT (Continue on reverse side if necessary and identify by block number) (lcb)
A numerical procedure is developed for a two-dimensional azimuthal (or planar) invariant form of the thin-layer Navier-Stokes equations. The governing equations are generalized over the usual two-dimensional and axisymmetric formulations by allowing non-zero velocity components in the azimuthal direction. The equations are solved with an implicit approximate factorization finite-difference scheme. Inviscid and viscous results are presented for both external and internal flows, for spinning and non-spinning bodies.

TABLE OF CONTENTS

LIST OF ILLUSTRATIONS

I. INTRODUCTION

The three-dimensional flow field equations are frequently simplified for flow fields which are invariant in one coordinate direction. For example, in axisymmetric problems the pressure, density, and properly chosen velocity components do not change in the circumferential direction. In the usual axisymmetric approximation the azimuthal velocity is assumed to be zero and the momentum equation in that direction can be eliminated. Thus, only four equations are required to be solved for four unknowns. However, for a variety of interesting flow fields the velocity component in the invariant direction (here taken as η) is not zero although the governing equations are still two-dimensional. Examples include axisymmetric swirl flows, the viscous flow about an infinitely swept wing, and the viscous flow about a spinning axisymmetric body at zero degrees angle of attack. Each of these flows can be solved as a two-dimensional problem although all three momentum equations have to be retained and source terms replace the derivative of the flux terms in the η direction.

In this paper the three dimensional thin-layer equations in general coordinates are presented. These equations are then reduced to a two dimensional set of equations which govern azimuthal invariant flows. The resulting η-invariant equations still allow arbitrary body shape in the remaining (ξ,ζ) directions and are solved with an implicit approximate factorization finite-difference scheme. Calculated results include flow about standard and hollow projectile shapes at zero angle of attack, flow over an infinitely swept wing, and an internal swirl flow with vortex breakdown.

II. GOVERNING EQUATIONS

The azimuthal-invariant equations are developed as a subset of the three-dimensional thin-layer Navier-Stokes equations. The basic formulation of the three-dimensional equations is developed in reference 1 and only the pertinent results are reviewed here.

A. Three-Dimensional Equations

The transformed three-dimensional thin-layer Navier-Stokes equations in non-dimensional and strong conservation law form are written as[1]

$$\partial_\tau \hat{q} + \partial_\xi \hat{E} + \partial_\eta \hat{F} + \partial_\zeta \hat{G} = Re^{-1} \partial_\zeta \hat{S} \tag{1}$$

---

1. *T. H. Pulliam and J. L. Steger, "On Implicit Finite-Difference Simulations of Three-Dimensional Flow", AIAA Paper No. 78-10, January 1978.*

where general coordinate transformations

$$\xi = \xi(x,y,z,t)$$

$$\eta = \eta(x,y,z,t)$$

$$\zeta = \zeta(x,y,z,t)$$

$$\tau = t$$

are used and

$$\hat{q} = J^{-1}\begin{bmatrix}\rho\\ \rho u\\ \rho v\\ \rho w\\ e\end{bmatrix} \qquad \hat{E} = J^{-1}\begin{bmatrix}\rho U\\ \rho uU + \xi_x p\\ \rho vU + \xi_y p\\ \rho wU + \xi_z p\\ (e+p)U - \xi_t p\end{bmatrix}$$

$$\hat{F} = J^{-1}\begin{bmatrix}\rho V\\ \rho uV + \eta_x p\\ \rho vV + \eta_y p\\ \rho wV + \eta_z p\\ (e+p)V - \eta_t p\end{bmatrix} \qquad \hat{G} = J^{-1}\begin{bmatrix}\rho W\\ \rho uW + \zeta_x p\\ \rho vW + \zeta_y p\\ \rho wW + \zeta_z p\\ (e+p)W - \zeta_t p\end{bmatrix}$$

$$\hat{S} = J^{-1}\begin{bmatrix} 0\\ \mu(\zeta_x^2+\zeta_y^2+\zeta_z^2)u_\zeta + (\mu/3)(\zeta_x u_\zeta+\zeta_y v_\zeta+\zeta_z w_\zeta)\zeta_x\\ \mu(\zeta_x^2+\zeta_y^2+\zeta_z^2)v_\zeta + (\mu/3)(\zeta_x u_\zeta+\zeta_y v_\zeta+\zeta_z w_\zeta)\zeta_y\\ \mu(\zeta_x^2+\zeta_y^2+\zeta_z^2)w_\zeta + (\mu/3)(\zeta_x u_\zeta+\zeta_y v_\zeta+\zeta_z w_\zeta)\zeta_z\\ \{(\zeta_x^2+\zeta_y^2+\zeta_z^2)[0.5\mu(u^2+v^2+w^2)_\zeta + \kappa Pr^{-1}(\gamma-1)^{-1}(a^2)_\zeta]\\ \quad + (\mu/3)(\zeta_x u+\zeta_y v+\zeta_z w)(\zeta_x u_\zeta+\zeta_y v_\zeta+\zeta_z w_\zeta)\}\end{bmatrix}$$

The velocities

$$\left.\begin{aligned} U &= \xi_t + \xi_x u + \xi_y v + \xi_z w \\ V &= \eta_t + \eta_x u + \eta_y v + \eta_z w \\ W &= \zeta_t + \zeta_x u + \zeta_y v + \zeta_z w \end{aligned}\right\} \qquad (2)$$

represent the contravarient velocity components.

The Cartesian velocity components (u,v,w) are retained as the dependent variables and are non-dimensionalized with respect to a_∞ (the free stream speed of sound). Pressure is defined as

$$p = (\gamma - 1)\ (e - .5\rho(u^2 + v^2 + w^2)) \qquad (3)$$

where γ is the ratio of specific heats, the density (ρ) is referenced to ρ_∞, and the total energy (e) is referenced to $\rho_\infty\ a_\infty^2$. The additional parameters are (κ) the coefficient of thermal conductivity, (μ) the dynamic viscosity, (Re) the Reynolds number, (Pr) the Prandtl number, and (λ) which through the Stokes hypothesis is $(-2/3)\mu$.

The metric terms of equation (1) are defined from

$$\begin{aligned} \xi_x &= J(y_\eta z_\zeta - y_\zeta z_\eta) & \eta_x &= J(z_\xi y_\zeta - y_\xi z_\zeta) \\ \xi_y &= J(z_\eta x_\zeta - x_\eta z_\zeta) & \eta_y &= J(x_\xi z_\zeta - x_\zeta z_\xi) \\ \xi_z &= J(x_\eta y_\zeta - y_\eta x_\zeta) & \eta_z &= J(y_\xi x_\zeta - x_\xi y_\zeta) \\ \zeta_x &= J(y_\xi z_\eta - z_\xi y_\eta) & \xi_t &= -x_\tau \xi_x - y_\tau \xi_y - z_\tau \xi_z \\ \zeta_y &= J(x_\eta z_\xi - x_\xi z_\eta) & \eta_t &= -x_\tau \eta_x - y_\tau \eta_y - z_\tau \eta_z \\ \zeta_z &= J(x_\xi y_\eta - y_\xi x_\eta) & \zeta_t &= -x_\tau \zeta_x - y_\tau \zeta_y - z_\tau \zeta_z \end{aligned} \qquad (4)$$

and

$$J^{-1} = x_\xi y_\eta z_\zeta + x_\zeta y_\xi z_\eta + x_\eta y_\zeta z_\xi - x_\xi y_\zeta z_\eta - x_\eta y_\xi z_\zeta - x_\zeta y_\eta z_\xi$$

The "thin-layer" approximation[1,2,3] used here requires that all body surfaces be mapped onto ζ = constant places and that Re >> 1. Essentially, all the viscous terms in the coordinate directions (here taken as ξ and η) along the body surface are neglected while terms in the ζ or the near normal direction to the body are retained. This approximation is used because, due to computer speed and storage limitations, fine grid spacing can only be provided in one coordinate direction (usually taken as the near normal direction) and the grid spacing available in the other two directions is usually too coarse to resolve the viscous terms.

B. η-Invariant Equations

The thin-layer azimuthal-invariant equations are obtained from the three dimensional equations by making use of two restrictions: (1) all body geometries are of an axisymmetric type; (2) the state variables and the contravariant velocities do not vary in the azimuthal direction. Here η is used for the azimuthal coordinate and the terms azimuthal and η-invariant will be used interchangeably. In what follows, the $\partial_\eta \hat{F}$ term of equation (1) shall be reduced to the source term of the η-invariant equations.

A sketch of a typical axisymmetric body is shown in Figure 1a. In order to determine the circumferential variation of typical flow and geometric parameters, we first establish correspondence between the inertial Cartesian coordinates (x,y,z) (to which the dependent variables are referenced), the natural inertial cylindrical coordinates (x,ϕ,R), and the transformed variables (ξ,η,ζ). The choice of the independent variables ξ, η, ζ is restricted, as shown in Figure 1c, insofar as η must vary as ϕ, i.e. $\phi = C\eta$ (where C is a constant). From the views shown in Figure 1, the relationship between the coordinate systems are observed to be

$$\left.\begin{aligned} \phi &= C\eta \\ x &= x(\xi,\zeta,\tau) \\ y &= R(\xi,\zeta,\tau)\sin\phi \\ z &= R(\xi,\zeta,\tau)\cos\phi \end{aligned}\right\} \qquad (5)$$

---

2. *J. L. Steger, "Implicit Finite Difference Simulation of Flow About Arbitrary Geometrics With Application to Airfoils", AIAA Paper No. 77-665, June 1977.*

3. *B. S. Baldwin and H. Lomax, "Thin Layer Approximation and Algebraic Model for Separated Turbulent Flows", AIAA Paper No. 78-257, January 1978.*

where $\phi = \phi(\tau)$ and the Cartesian and cylindrical coordinates are related in the usual way. Note that x and R are general functions of only ξ, ζ, and τ.

To evaluate the metric terms needed in Equation (1) we first form

$$\left.\begin{aligned} x_\xi &= x_\xi & y_\xi &= R_\xi \sin\phi \\ x_\eta &= 0 & y_\eta &= \phi_\eta R\cos\phi \\ x_\zeta &= x_\zeta & y_\zeta &= R_\zeta \sin\phi \\ z_\xi &= R_\xi \cos\phi & x_\tau &= x_\tau \\ z_\eta &= -\phi_\eta R\sin\phi & y_\tau &= R_\tau \sin\phi + \phi_\tau R\cos\phi \\ z_\zeta &= R_\zeta \cos\phi & z_\tau &= R_\tau \cos\phi - \phi_\tau R\sin\phi \end{aligned}\right\} \quad (6)$$

and substitute these relations into equation (4) which results in

$$\left.\begin{aligned} \xi_x &= J\phi_\eta R R_\zeta & \eta_x &= 0 \\ \xi_y &= J\phi_\eta R x_\zeta \sin\phi & \eta_y &= \cos\phi/(\phi_\eta R) \\ \xi_z &= -J\phi_\eta R x_\zeta \cos\phi & \eta_z &= -\sin\phi/(\phi_\eta R) \\ \zeta_x &= -J\phi_\eta R R_\xi & \xi_t &= J\phi_\eta R(x_\zeta R_\tau - x_\tau R_\zeta) \\ \zeta_y &= J\phi_\eta R x_\xi \sin\phi & \eta_t &= -\phi_\tau/\phi_\eta \\ \zeta_z &= J\phi_\eta R x_\xi \cos\phi & \zeta_t &= J\phi_\eta R(x_\tau R_\xi - R_\tau x_\xi) \end{aligned}\right\} \quad (7)$$

with

$$J^{-1} = R\phi_\eta(x_\xi R_\zeta - x_\zeta R_\xi) \quad .$$

Once the term $\partial_\eta \hat{F}$ is evaluated in equation (1) we can eliminate the cylindrical coordinates altogether by letting $\phi = 0$ so that $R = z$ (see

Figure 1), $\sin\phi = 0$ and $\cos\phi = 1$. The term ϕ_η is simply the scaling constant, C, between η and ϕ.

Equations (2) and (7) can be used to obtain the Cartesian velocity components in terms of the metrics and contravariant velocities

$$\begin{bmatrix} u \\ v \\ w \end{bmatrix} = \begin{bmatrix} x_\xi & 0 & x_\zeta \\ R_\xi \sin\phi & R\phi_\eta \cos\phi & R_\zeta \sin\phi \\ R_\xi \cos\phi & -R\phi_\eta \sin\phi & R_\zeta \cos\phi \end{bmatrix} \begin{bmatrix} U - \xi_t \\ V - \eta_t \\ W - \zeta_t \end{bmatrix} \tag{8}$$

The contravariant velocities, U, V, and W are required to be invariant in η and the metric terms ξ_t, η_t, and ζ_t are zero for steady flows and are invariant in η for such unsteady body motions as axial acceleration or axisymmetric spinning.

The resulting expressions for u,v,w and the metrics, equation (7), have only $\sin\phi$ and $\cos\phi$ variation in the η-direction. Consequently, equations (7) and (8) can now be used in equation (1) to reduce the η derivative of the flux vector, $\hat{F}$. Taking, for example, the third term of the flux vector $\hat{F}$

$$\rho v V + \eta_y p$$

and evaluating its η derivative results in

$$\rho V \frac{\partial v}{\partial \eta} + p \frac{\partial (\eta_y)}{\partial \eta} = \rho V \phi_\eta \left[R_\xi (U - \xi_t) \cos\phi \right.$$

$$\left. - R\phi_\eta^2 (V - \eta_t) \sin\phi + R_\zeta (W - \zeta_t) \cos\phi \right] - p \sin\phi / R \tag{9}$$

The remaining terms of $\partial_\eta \hat{F}$ are similarly determined and result in the following source term

$$\hat{H} = J^{-1}\phi_\eta \begin{bmatrix} 0 \\ 0 \\ \rho V[R_\xi(U-\xi_t)\cos\phi - R\phi_\eta(V-\eta_t)\sin\phi \\ \quad + R_\zeta(W-\zeta_t)\cos\phi] - p\sin\phi/(R\phi_\eta) \\ -\rho V[R_\xi(U-\xi_t)\sin\phi + R\phi_\eta(V-\eta_t)\cos\phi \\ \quad + R_\zeta(W-\zeta_t)\sin\phi] - p\cos\phi/(R\phi_\eta) \\ 0 \end{bmatrix} \tag{10}$$

Since the solution based on the above restrictions will be independent of ϕ, equation (10) can be evaluated at $\phi = 0$ without loss of generality. The resulting thin-layer η-invariant equations are then written as

$$\partial_\tau \hat{q} + \partial_\xi \hat{E} + \partial_\zeta \hat{G} + \hat{H} = Re^{-1}\partial_\zeta \hat{S} \tag{11}$$

with the metrics and Cartesian velocities in $\hat{q}$, $\hat{E}$, $\hat{G}$, and $\hat{S}$ of equation (1) evaluated at $\phi = 0°$, and

$$\hat{H} = J^{-1}\phi_\eta \begin{bmatrix} 0 \\ 0 \\ \rho V[R_\xi(U-\xi_t) + R_\zeta(W-\zeta_t)] \\ -\rho V R\phi_\eta(V-\eta_t) - p/(R\phi_\eta) \\ 0 \end{bmatrix} \tag{12}$$

Equation (11) contains only two spatial derivatives but does retain all three momentum equations thus allowing a degree of generality over the standard axisymmetric equations. In particular, the circumferential velocity is not assumed to be zero. We remark that retaining all three momentum equations to compute crossflow components, such as swirl velocity, is not a noval idea; however, the form of the equations presented here is more general than what we have previously encountered.

C. Surface Boundary Conditions

For inviscid flow, the tangency condition is expressed as $W = 0$ along the body surface, ζ = constant. A relation for pressure on the body surface is obtained by combining the three transformed momentum equations and making use of the η-invariant assumptions

$$p_n(\zeta_x^2 + \zeta_z^2) = (\xi_x\zeta_x + \xi_z\zeta_z)p_\xi + (\zeta_x^2 + \zeta_z^2)p_\zeta =$$

$$\rho[\partial_\tau\zeta_t + u\partial_\tau\zeta_x + v(J\phi_\eta Rx_\xi\phi_\tau) + w\partial_\tau(J\phi_\eta Rx_\xi)] \qquad (13)$$

$$- \rho U(\zeta_x u_\xi + \zeta_z w_\xi) + \rho V[Jx_\xi R^2\phi_\eta{}^3(V-\eta_t)]$$

where p_n is the normal pressure gradient at the body surface.

The no slip boundary conditions for viscous flow is enforced by setting

$$U = V = W = 0 \qquad (14)$$

where as usual it is assumed that the ξ, η, ζ coordinates are referenced to the body. However, for an axisymmetric body spinning with angular velocity ω, we have the choice of keeping the ξ, η, ζ coordinates fixed in space and allowing the body to slide under the ζ = constant boundary surface. In this case the no slip condition would be

$$U = W = 0 \qquad \text{and} \qquad V = \omega \qquad (15)$$

Otherwise, for a spinning body the usual no slip condition, equation (14), would be imposed with $\eta_t = -\phi_\eta\omega$.

Once the contravariant velocities (U,V, and W) are specified at the body, the Cartesian velocities (u, v, and w) can be found from either equation (8) (with $\phi = 0°$) or from

$$\begin{bmatrix} u \\ v \\ w \end{bmatrix} = J^{-1} \begin{bmatrix} \eta_y\zeta_z & 0 & -\eta_y\xi_z \\ 0 & (\xi_x\zeta_z - \xi_z\zeta_x) & 0 \\ -\eta_y\zeta_x & 0 & \eta_y\xi_x \end{bmatrix} \begin{bmatrix} U-\xi_t \\ V-\eta_t \\ -\zeta_t \end{bmatrix} \qquad (16)$$

D. Turbulent Viscosity Model

The turbulence model used in the program is that due to Cebeci but modified by Baldwin and Lomax[3]. The Prandtl-Van Driest formulation of the inner eddy viscosity model requires the calculation of the vorticity

$$|\omega_v| = \sqrt{\left(\frac{\partial u}{\partial y} - \frac{\partial v}{\partial x}\right)^2 + \left(\frac{\partial v}{\partial z} - \frac{\partial w}{\partial y}\right)^2 + \left(\frac{\partial w}{\partial x} - \frac{\partial u}{\partial z}\right)^2} \tag{17}$$

Again, utilizing the relationships developed earlier, the vorticity term in transformed coordinates reduces to

$$\omega_v^2 = \left(\frac{\partial \xi}{\partial x}\frac{\partial v}{\partial \xi} + \frac{\partial \zeta}{\partial x}\frac{\partial v}{\partial \zeta}\right)^2 + \left(\frac{\partial \xi}{\partial z}\frac{\partial v}{\partial \xi} + \frac{\partial \zeta}{\partial z}\frac{\partial v}{\partial \zeta} - \frac{\partial \eta}{\partial y}\frac{\partial w}{\partial \eta}\right)^2 + \left[\left(\frac{\partial \xi}{\partial x}\frac{\partial w}{\partial \xi} + \frac{\partial \zeta}{\partial x}\frac{\partial w}{\partial \zeta}\right) - \left(\frac{\partial \xi}{\partial z}\frac{\partial u}{\partial \xi} + \frac{\partial \zeta}{\partial z}\frac{\partial u}{\partial \zeta}\right)\right]^2 \tag{18}$$

III. NUMERICAL ALGORITHM

A fully implicit, approximately factored, finite difference algorithm in the delta form as analyzed by Beam and Warming[4] is used here. If the flow field conditions permit, the use of an implicit scheme can allow larger time steps over an explicit scheme. Overly restrictive explicit stability limits can be encountered with the fine grids required for flow resolution in viscous regions or in the vicinity of abrupt geometry changes.

The finite difference algorithm can be first or second order accurate in time and second or fourth order accurate in space. The solution of the two-dimensional system of difference equations is implemented by an approximate factorization of the equations into two one-dimensional-like systems of equations. This procedure has been utilized in previous applications[1-3,5] similar to ours, and the bibliographies of references 1-5 should be referred to for numerous related works.

---

4. *R. Beam and R. F. Warming, "An Implicit Factored Scheme for the Compressible Navier-Stokes Equations", AIAA Paper No. 77-645, June 1977.*

5. *P. Kutler, S. R. Chakravarthy, and C. K. Lombard, "Supersonic Flow Over Ablated Nose Tips Using an Unsteady Implicit Numerical Procedure", AIAA Paper No. 78-213, January 1978.*

A. Finite Difference Equations

The resulting finite difference equations, written in delta form are

$$(I+h\delta_\xi \hat{A}^n - \varepsilon_I J^{-1}\nabla_\xi\Delta_\xi J)\ (I+h\delta_\zeta \hat{C}^n - \varepsilon_I J^{-1}\nabla_\zeta\Delta_\zeta J$$

$$- hRe^{-1}\delta_\zeta J^{-1}\hat{M}^n J)\ x\ (\hat{q}^{n+1}-\hat{q}^n) = -\Delta t(\delta_\xi \hat{E}^n + \delta_\zeta \hat{G}^n \qquad (19)$$

$$- Re^{-1}\delta_\zeta \hat{S}^n) - \Delta t\hat{H}^n - \varepsilon_E J^{-1}\ [(\nabla_\xi\Delta_\xi)^2 + (\nabla_\zeta\Delta_\zeta)^2]\ J\hat{q}^n$$

Here $h = \Delta t$ because only first order accuracy in the time differencing is needed for the steady and quasi-steady state flows which are considered in this paper. The δ's represent second or fourth order central spatial difference operators[1,2], with Δ and ∇ the conventional forward and backward differences, respectively. The Jacobian matrices $\hat{A} = \frac{\partial \hat{E}}{\partial \hat{q}}$, $\hat{C} = \frac{\partial \hat{G}}{\partial \hat{q}}$ along with the coefficient matrix M obtained from the local time linearization of S are described in detail in reference 1. Fourth order explicit (ε_E) and implicit (ε_I) numerical dissipation terms are incorporated into the differencing scheme to control nonlinear instabilities. A typical range for the smoothing coefficients is ε_E = (1 to 5) Δt with $\varepsilon_I = 2\ \varepsilon_E$.

B. Numerical Implementation of Boundary Conditions

For inviscid flow updated values of $\hat{q}$ are obtained along the body surface by linear extrapolation of ρ, U, and V. In viscous flow U, V, and W are specified and we typically set $\rho_\zeta = 0$. Once the contravariant velocities are specified, equation (16) is solved for u, v, and w along the body surface. Pressure is obtained from numerical integration of equation (13). The axis singularity is handled as in reference 1, where flow variables are not required at the axis due to the fact that the required flux vectors are zero on the singularity. Extrapolated outflow conditions are applied although pressure is often fixed at the back boundary for subsonic flow. All boundary conditions are treated explicitly.

IV. RESULTS

The η-invariant equations are applied to a number of axisymmetric and planar type flow problems. Although the usual two-dimensional equations[5] would be more appropriate for simple non-spinning axisymmetric bodies, we began, nevertheless, to verify the η-invariant code by computing conventional axisymmetric flows. It happens that some of the axisymmetric results are interesting by themselves, specifically the hollow projectile solutions, and various calculations are presented to show the versatility of the numerical algorithm with its general geometry capability. Viscous flow results for spinning projectiles and an infinite swept wing are included to show the utility of the η-invariant assumptions. Finally, an inviscid internal swirl flow with vortex breakdown is investigated. In all cases the same basic code was used with only minor modifications of the boundary conditions.

A. Standard Projectile

In order to verify the η-invariant code, an inviscid flow about a typical projectile shape was investigated. The inviscid solution was obtained for a 3 caliber (i.e. 3 maximum body diameters) ogive nose, 2 caliber center body and 1 caliber 7° boattail at $M_\infty = .95$ and zero angle of attack. The calculated pressure coefficient is compared in Figure 2 with the results obtained from an inviscid three dimensional small disturbance program for projectile-like flow fields, developed by Reklis, et al[6]. The two results are in good agreement and clearly show the same shock patterns, both near the nose-cylinder and cylinder-boattail junctions. The grid for our calculations contained 60 longitudinal points in ξ, with clustering at the boattail, and 25 points in the radial (ζ) direction, with exponential stretching away from the body.

For viscous flow calculations the original projectile grid was refined to 40 points in the ζ-direction to obtain a very fine mesh near the body. The computed C_p distribution for laminar flow and free stream Reynolds number of 0.5×10^6 (based on body diameter) is shown in Figure 3, together with the previous inviscid results. In the viscous flow the expansion and subsequent shock at the nose-cylinder junction are reduced, and the flow separates and reattaches on the boattail. As with the inviscid calculation, the wake of the viscous case was modeled as an attached sting.

A major motivation for the development of the η-invariant code was to obtain the capability to compute flow fields about spinning projectile shapes. Results presented in Figure 4 show the boundary layer profiles obtained for the projectile when spun at a representative non-dimensional spin parameter of $\omega D/U_\infty = 0.11$. The body geometry and

---

6. *R. P. Reklis, W. B. Sturek, and F. R. Bailey, "Computation of Transonic Flow Past Projectiles at Angle of Attack", AIAA Paper No. 78-1182, July 1978.*

viscous flow conditions are the same as for the previous case, while ω is the angular velocity and D is the maximum body diameter. For the specified Mach number of M_∞ = .95 this spin parameter would correspond to a 105 millimeter diameter projectile spinning at a rate of 2,900 rev/min. The surface pressure distributions were practically identical for the spinning and non-spinning cases and even the streamwise velocity profile was essentially unaffected by the addition of this amount of spin. These results are substantiated in part by experimental data obtained by Kayser[7].

B. Hollow Projectile

Of current interest in shell design is the utilization of hollow projectiles which can be made to fly "flat" trajectories. Hollow projectiles can be considered as tubular or ring airfoils and must be spun in order to achieve in-flight stability.

A series of computations about hollow projectile-like shapes at zero angle of attack were made to demonstrate the capability of the η-invariant code to calculate crossflow velocity components and general geometry shapes. The specific shape used for the computations was generated from a conventional NACA 64A006 airfoil rotated about a symmetry axis to form an axisymmetric cowl or ring airfoil as shown in Figure 5. The airfoil grid generation program of Sorenson and Steger[8] was used to form the computational mesh.

Inviscid flow results are presented in Figures 6a, b, c, d, and e for M_∞ = 0.6, 0.7, 0.8, 0.9, and 1.2. In all cases the pressure distribution is plotted for the internal and external surfaces. The flow remains totally subsonic for M_∞ = 0.6 and as the free stream Mach number is increased the flow becomes choked at the throat with a shock standing inside (Figure 6b). As the free stream Mach number is further increased the internal shock moves to the trailing edge (Figures 6c and 6d). At M_∞ = 1.2 a standing bow shock is formed in front of the tubular airfoil as shown in Figure 7. The solid line indicates the bow shock and the dashed lines represents the sonic line. A plot of the pressure distribution along the axis is also shown for this case in Figure 8.

---

7. *L. D. Kayser, U.S. Army Ballistic Research Laboratory, Aberdeen Proving Ground, Maryland. Private communication.*

8. *R. Sorensen and J. L. Steger, "Simplified Clustering of Nonorthogonal Grids Generated by Elliptic Partial Differential Equations", NASA TM 73252.*

Prior to spinning the projectile, a viscous, turbulent thin layer solution was calculated at $M_\infty = 0.8$ for comparison to the inviscid flow. In the viscous flow the shock wave moves back from the trailing edge, and a small separation bubble forms at the foot of the shock, as indicated in Figure 9.

A spinning solution was obtained for the same shape at $M_\infty = 0.8$, zero angle of attack, and with a spin parameter $\omega D/U_\infty = 0.11$. The velocity profiles are presented in Figure 10 at an external position of $x/c = .33$. As for the standard projectile, the v component of velocity shown here decreases from a maximum value at the surface to effectively zero at the edge of the boundary layer. The pressure distributions were also unchanged between the spinning and non-spinning cases.

C. Infinite Swept Wing

The flow about an infinitely swept wing is another well known example of an η-invariant flow where the η coordinate is chosen parallel to the wing leading edge as shown in Figure 11a. For inviscid flow one can use simple sweep theory to convert the flow over an infinitely swept wing into a conventional two dimensional airflow problem. In viscous flow, however, one finds that the streamlines over the wing are curved, hence the cross flow momentum equation must be retained (see references 9 and 10 for representative boundary layer procedures).

The η-invariant equations for an infinitely swept wing are most easily obtained by considering this problem as a limiting case of the hollow projectile. From this point of view we consider the flow about a ring airfoil with $R \to \infty$ and $\phi_\eta \to 0$. As $R \to \infty$ and $\phi_\eta \to 0$, the term $R\phi_\eta \to 1$ and the entire source term $H \to 0$, see equation (12).

A turbulent calculation at $Re = 20 \times 10^6$ about a NACA 0010 cross sectional wing with 45° sweep, $\alpha = 0°$, and $M_\infty = 0.85$ is compared with an inviscid small perturbation solution obtained with the Bailey-Ballhaus[11] three dimensional wing program as shown in Figure 11b.

---

9. *A. Mager, "Theory of Laminar Flows", Vol. IV, High Speed Aerodynamics and Jet Propulsion, F. K. Moore, ed., Princeton University Press, Princeton, New Jersey, 1964.*

10. *F. A. Dvorak and F. A. Woodward, "A Viscous/Potential Flow Interaction Analysis Method for Multi-Element Infinite Swept Wings", Vol. 1, NASA CR-2476, November 1974.*

11. *F.R. Bailey and W. F. Ballhaus, "Comparison of Computed and Experimental Pressures for Transonic Flow About Isolated Wings and Wing-Fuselage Configurations", NASA CP-347, March 1975.*

(While an inviscid two-dimensional airfoil program could have been used for this comparison, the three-dimensional result was available from another application.) For this case viscous effects are somewhat mild, but even so, a discrepancy between the inviscid and viscous solution is evident from the trailing edge up to approximately the mid-chord.

D. Internal Swirl Flow

As a final application of the η-invariant equations we have undertaken preliminary calculations to simulate the inviscid vortex breakdown of an internal swirling jet flow. After an axisymmetric vortex flow bursts, the flow field may remain essentially axisymmetric or it may spiral in a non-axisymmetric manner (see Hall[12] or Leibovich[13] for interesting review articles). Of course, only axisymmetric flows can be properly simulated with the η-invariant equations.

In our preliminary calculations we have attempted an inviscid simulation of the experimental measurements due to Garg[14]. Garg studied the breakdown of a swirl flow in an expanding axisymmetric channel which has an inlet radius of 1.905 cm and which expands to 2.54 cm over an axial distance of 25.4 cm. The circular channel then continues on with the maximum radius of 2.54 cm for another 35 cm. The measured initial velocities were least squares fit and in our simulations we chose Garg's first case

$$u = 23.8\ (1 + 1.581\ e^{-8.92\ z^2}) \qquad \text{(cm/sec)}$$

$$v = 20.2\ (1 - e^{-8.92\ z^2})\ /\ z \qquad \text{(cm/sec)}$$

---

12. *M. G. Hall, "Vortex Breakdown", Annual Review of Fluid Mechanics, Vol. 4, Annual Reviews, Inc., Palo Alto, California, 1972.*

13. *S. Leibovich, "The Structure of Vortex Breakdown", Annual Review of Fluid Mechanics, Vol. 10, Annual Reviews, Inc., Palo Alto, California, 1978.*

14. *A. K. Garg, "Oscillatory Behavior in Vortex Breakdown Flows: An Experimental Study Using a Laser Doppler Anemometer", MS Thesis, Cornell University, Ithaca, New York, 1977.*

In the experiment, which was conducted in water, this case exhibits an axisymmetric bubble type breakdown with an axial stagnation point at approximately 2.3 cm downstream of the inlet (x = 0.0). In the numerical simulation the initial velocity profiles were scaled to put u at the outer wall in a Mach number range of M = 0.2. The axial core has a higher Mach number and some compressibility effects are observed in our calculations.

Results of the numerical simulation are presented in Figures 12 through 14. In Figure 12, axial (solid line) and circumferential (dashed line) velocity profiles are displayed for different axial locations. The axial jet flow and vortex profile at the initial station (x = 0.2 cm) are shown in Figure 12a. The axial flow decelerates and the vortex weakens in Figures 12b and 12c. Stagnation occurs at approximately x = 2 cm, which compares with an experimental value of x = 2.1 cm station, Figure 12d, while further downstream a strong reversed jet is observed, Figure 12e. Velocity vectors are shown in Figure 13 from x = 0.2 cm to x = 3.6 cm. The region of reversed flow continues downstream to the end of the tube.

Pressure along the centerline of the axisymmetric channel is shown in Figure 14. The large adverse pressure gradient occurs right at breakdown. It should be pointed out that pressure was allowed to float at both ends of the tube, i.e. $p_x = 0$ at inflow and outflow. Fixing pressure at the inlet leads to an inconsistency, and, if pressure is arbitrarily fixed at outflow, a pressure wave propagates back and forth through the channel. Because pressure is not specified, the computed pressure field is not unique. However, the velocity field does appear to be unique. In a numerical experiment we added a constant to the pressure field shown in Figure 14. The steady state velocity field remained essentially unchanged as the equations were then integrated further in time. If the flow were truly incompressible, $a_\infty \to \infty$, any constant could have been added to the pressure field (and boundaries) without changing the velocity field.

V. CONCLUSIONS

A versatile azimuthal-invariant version of the thin layer Navier-Stokes equations has been developed. Because of its general geometry capability, the same code has been used to compute the flow for standard and hollow projectile shapes, an infinitely swept wing, and internal swirl flows. Since the η-invariant code is a subset of the full three-dimensional version it can also be utilized as a relatively inexpensive tool for numerical algorithm development with subsequent implementation to the three-dimensional version.

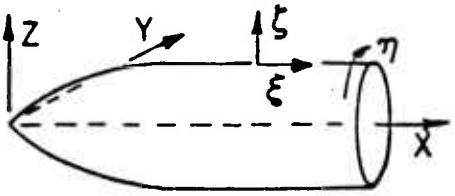

PROJECTILE-TYPE BODY
(a)

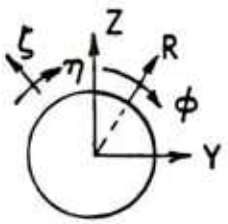

X = CONST. PLANE
(b)

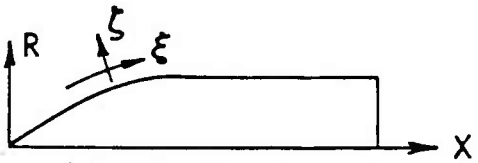

ϕ = CONST. PLANE
(c)

$$\phi = C_\eta$$
$$X = X(\xi,\zeta,\tau)$$
$$Y = R(\xi,\zeta,\tau)\sin\phi$$
$$Z = R(\xi,\zeta,\tau)\cos\phi$$

Figure 1. Axisymmetric Body and Coordinate System

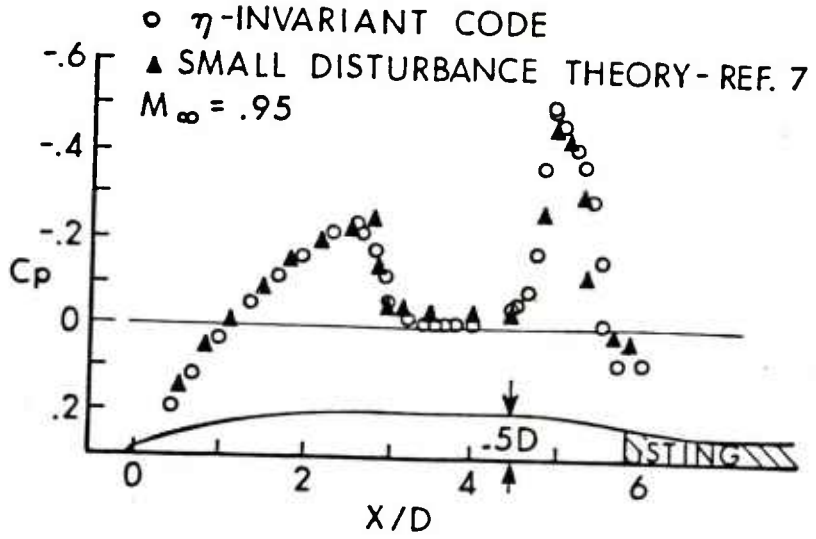

Figure 2. Inviscid Transonic Flow Over an Ogive-Cylinder-Boattail Body

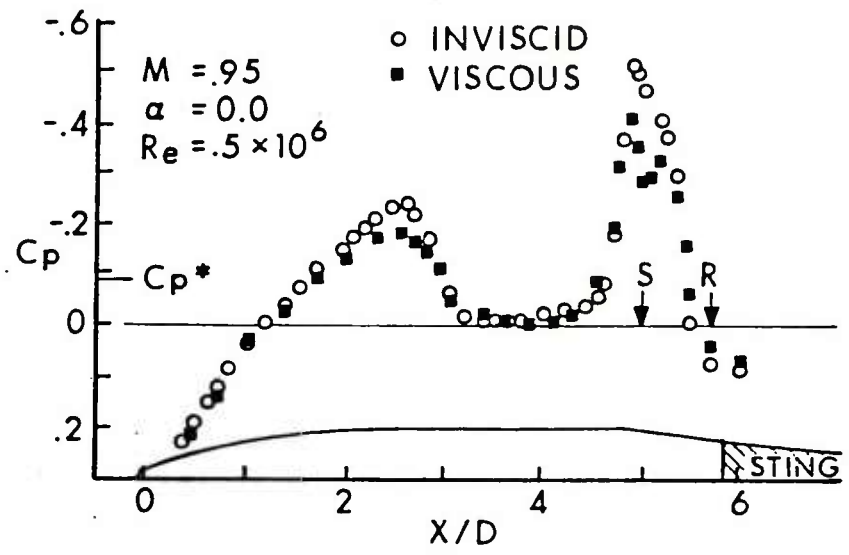

Figure 3. Viscous Effect on Projectile Body

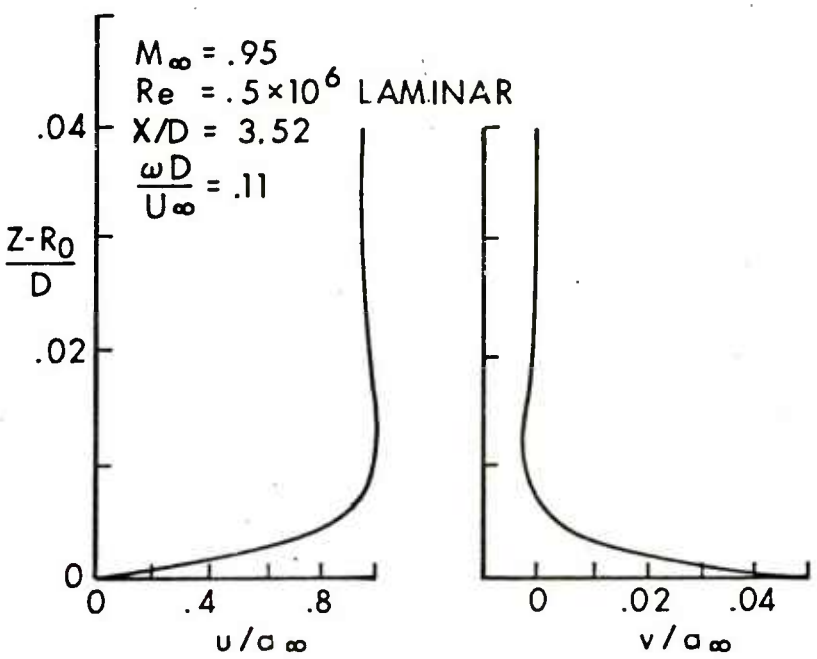

Figure 4. Velocity Profile for Spinning Projectile

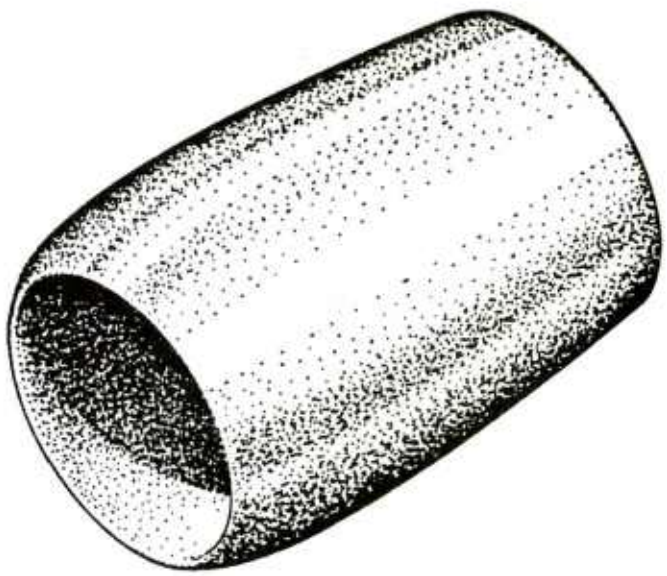

Figure 5. Hollow Projectile

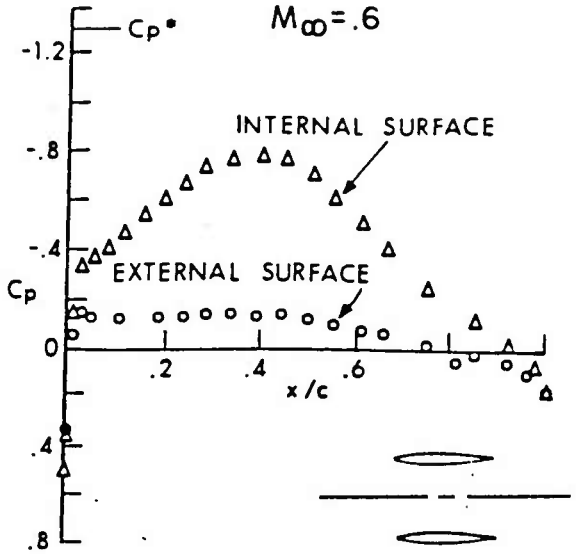

Figure 6a. Inviscid Transonic Flow Over Hollow Projectile, M_∞ = .6

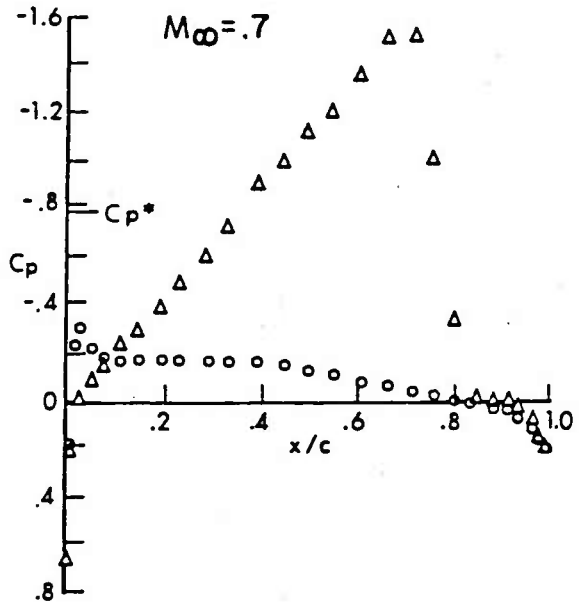

Figure 6b. Inviscid Transonic Flow Over Hollow Projectile, M_∞ = .7

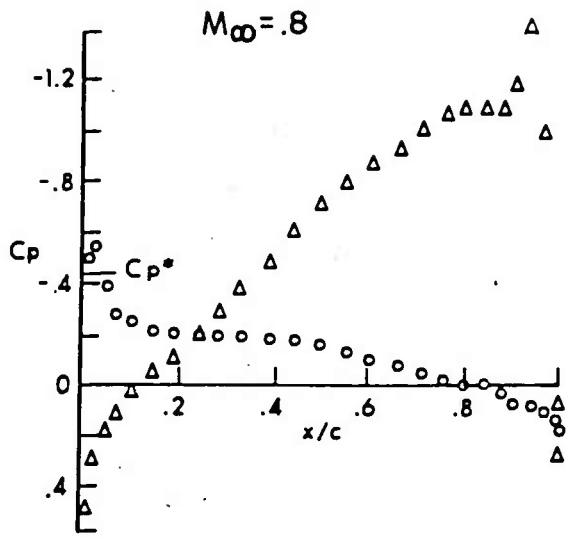

Figure 6c. Inviscid Transonic Flow Over Hollow Projectile, M_∞ = .8

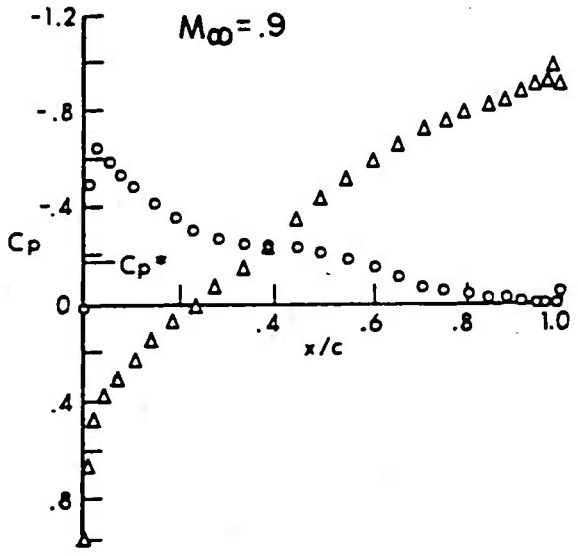

Figure 6d. Inviscid Transonic Flow Over Hollow Projectile, M_∞ = .9

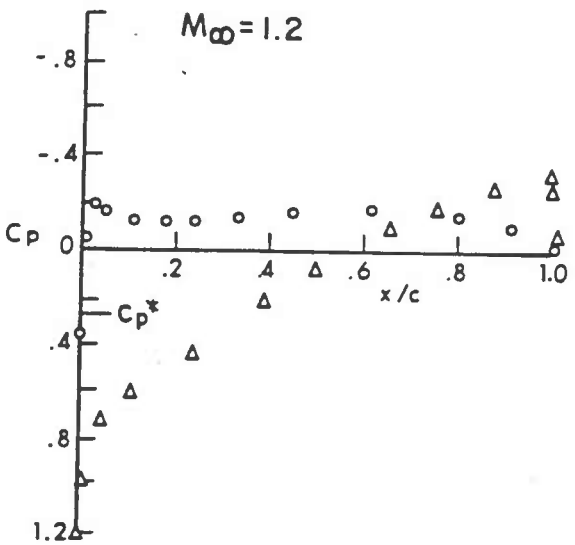

Figure 6e. Inviscid Transonic Flow Over Hollow Projectile, $M_\infty = 1.2$

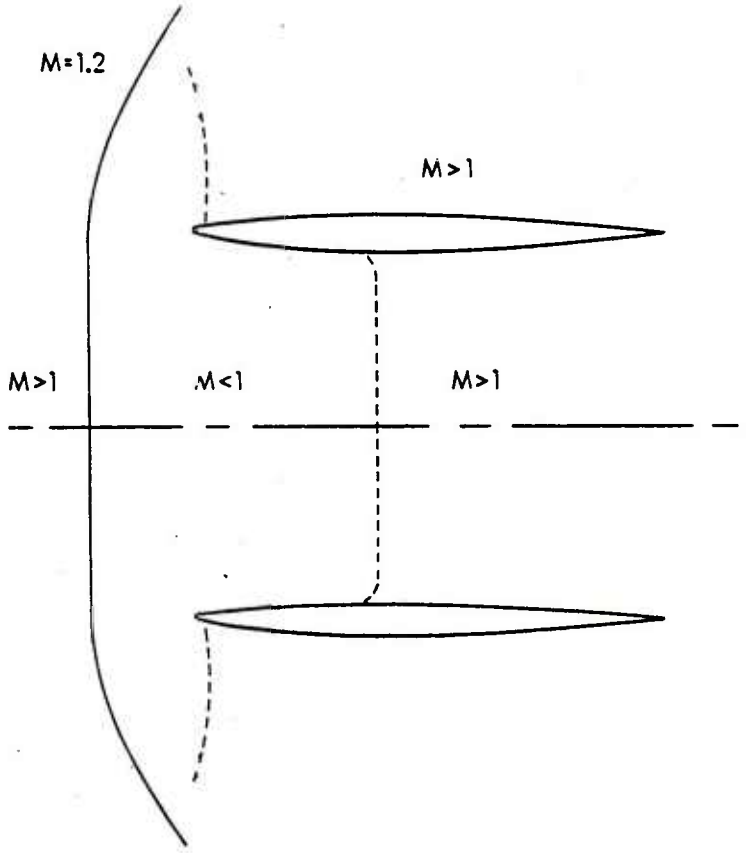

Figure 7. Shock Position and Sonic Line, M_∞ = 1.2

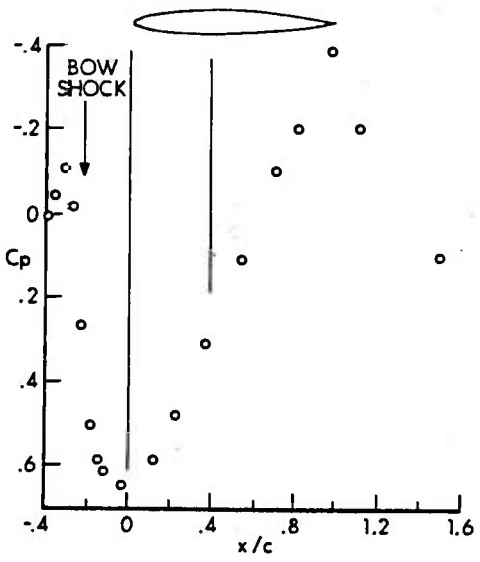

Figure 8. C_p Alorg Axis of Hollow Projectile, M_∞ = 1.2

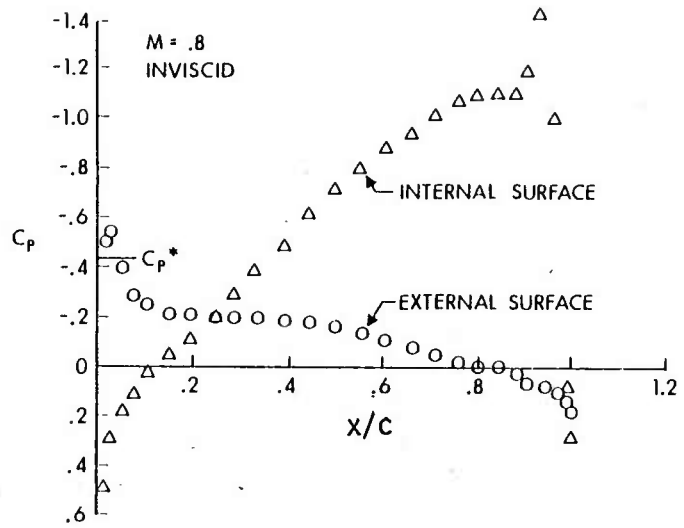

Figure 9. Viscous Transonic Flow Over Hollow Projectile, M_∞ = .8

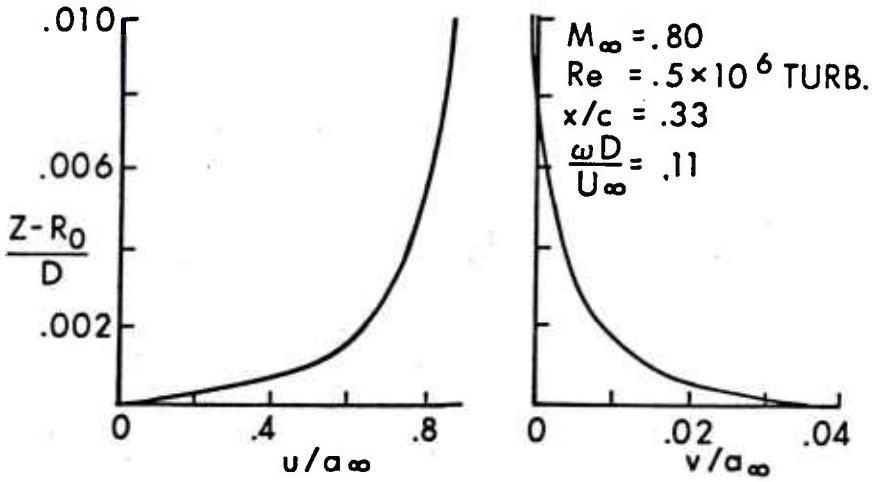

Figure 10. Velocity Profiles for Spinning Hollow Projectile

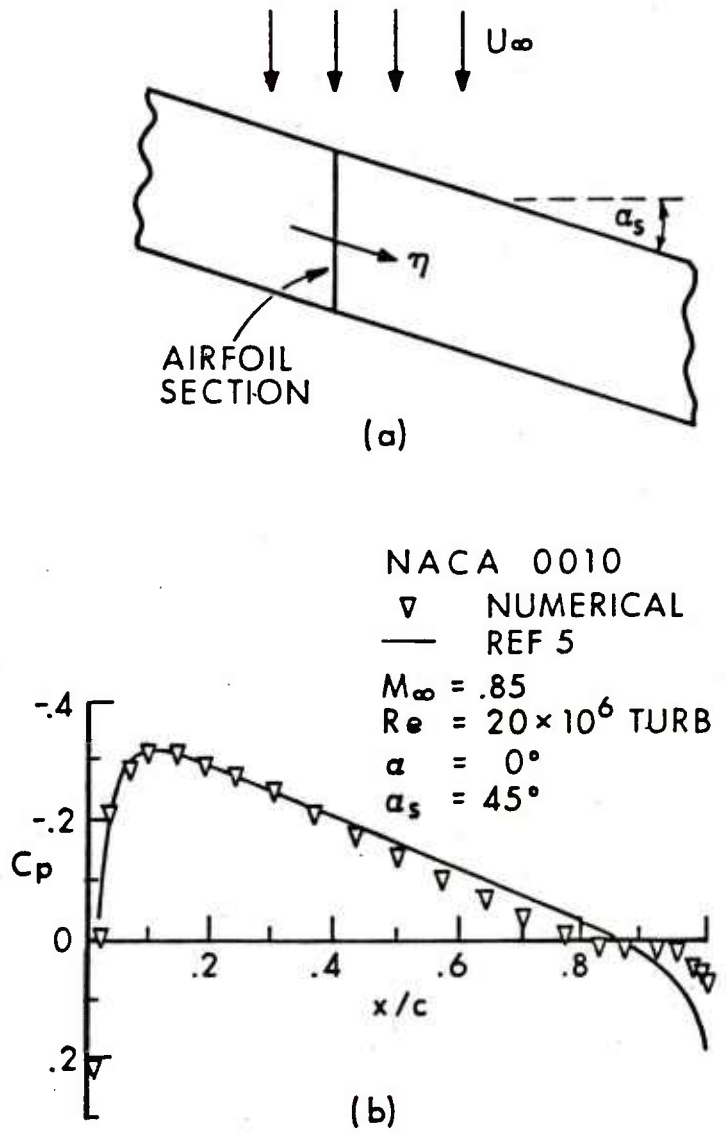

Figure 11. Infinite Swept Wing

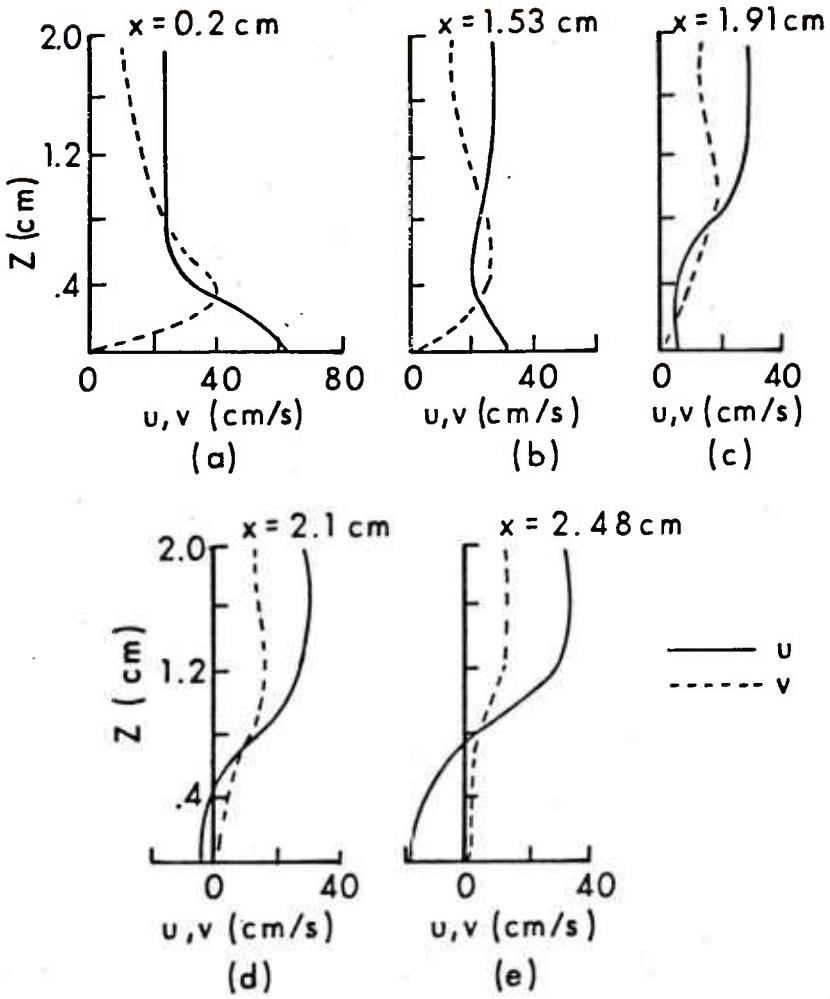

Figure 12. Velocity Profiles for Swirl Flow

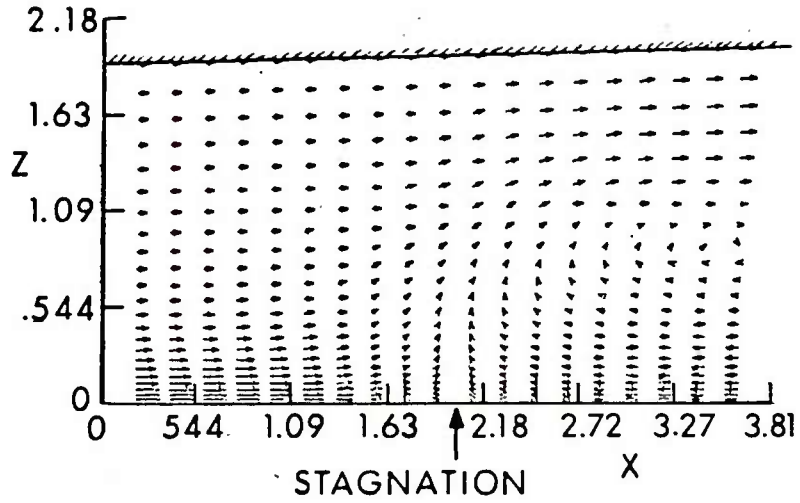

Figure 13. Velocity Vectors for Swirl Flow

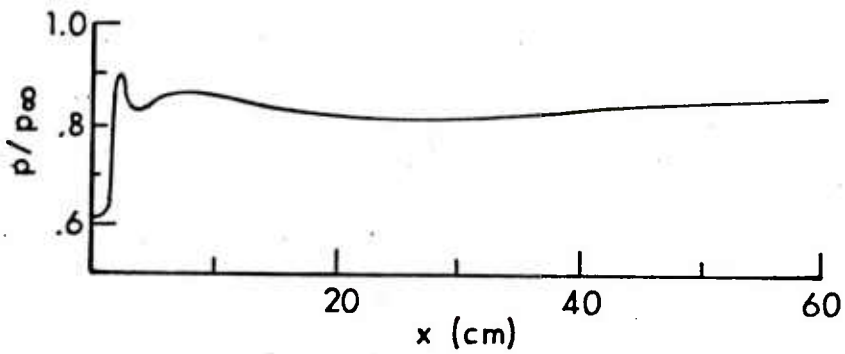

Figure 14. Pressure Along Centerline, z = 0

REFERENCES

1. T. H. Pulliam and J. L. Steger, "On Implicit Finite-Difference Simulations of Three-Dimensional Flow", AIAA Paper No. 78-10, January 1978.

2. J. L. Steger, "Implicit Finite Difference Simulation of Flow About Arbitrary Geometrics With Application to Airfoils", AIAA Paper No. 77-665, June 1977.

3. B. S. Baldwin and H. Lomax, "Thin Layer Approximation and Algebraic Model for Separated Turbulent Flows", AIAA Paper No. 78-257, January 1978.

4. R. Beam and R. F. Warming, "An Implicit Factored Scheme for the Compressible Navier-Stokes Equations", AIAA Paper No. 77-645, June 1977.

5. P. Kutler, S. R. Chakravarthy, and C. K. Lombard, "Supersonic Flow Over Ablated Nose Tips Using an Unsteady Implicit Numerical Procedure", AIAA Paper No. 78-213, January 1978.

6. R. P. Reklis, W. B. Sturek, and F. R. Bailey, "Computation of Transonic Flow Past Projectiles at Angle of Attack", AIAA Paper No. 78-1182, July 1978.

7. L. Kayser, U.S. Army Ballistic Research Laboratory, Aberdeen Proving Ground, Maryland. Private communication.

8. R. Sorensen and J. L. Steger, "Simplified Clustering of Nonorthogonal Grids Generated by Elliptic Partial Differential Equations", NASA TM 73252.

9. A. Mager, "Theory of Laminar Flows", Vol. IV, High Speed Aerodynamics and Jet Propulsion, F. K. Moore, ed., Princeton University Press, Princeton, New Jersey, 1964.

10. F. A. Dvorak and F. A. Woodward, "A Viscous/Potential Flow Interaction Analysis Method for Multi-Element Infinite Swept Wings", Vol. 1, NASA CR-2476, November 1974.

11. F. R. Bailey and W. F. Ballhaus, "Comparison of Computed and Experimental Pressures for Transonic Flow About Isolated Wings and Wing-Fuselage Configurations", NASA CP-347, March 1975.

12. M. G. Hall, "Vortex Breakdown", Annual Review of Fluid Mechanics, Vol. 4, Annual Reviews, Inc., Palo Alto, California, 1972.

13. S. Leibovich, "The Structure of Vortex Breakdown", Annual Review of Fluid Mechanics, Vol. 10, Annual Reviews, Inc., Palo Alto, California, 1978.

14. A. K. Garg, "Oscillatory Behavior in Vortex Breakdown Flows: An Experimental Study Using a Laser Doppler Anemometer", MS Thesis, Cornell University, Ithaca, New York, 1977.

DISTRIBUTION LIST

No. of Copies	Organization
12	Commander Defense Technical Info Center ATTN: DDC-DDA Cameron Station Alexandria, VA 22314
1	Commander US Army Materiel Development and Readiness Command ATTN: DRCDMD-ST 5001 Eisenhower Avenue Alexandria, VA 22333
8	Commander US Army Armament Research and Development Command ATTN: DRDAR-TSS (2 cys) DRDAR-LCA-F Mr. D. Mertz Mr. E. Falkowski Mr. A. Loeb Mr. R. Kline Mr. S. Kahn Mr. S. Wasserman Dover, NJ 07801
1	Commander US Army Armament Materiel Readiness Command ATTN: DRSAR-LEP-L Rock Island, IL 61299
1	Director US Army ARRADCOM Benet Weapons Laboratory ATTN: DRDAR-LCB-TL Watervliet, NY 12189
1	Commander US Army Aviation Research and Development Command ATTN: DRSAV-E P. O. Box 209 St. Louis, MO 63166
1	Director US Army Air Mobility Research and Development Laboratory Ames Research Center Moffett Field, CA 94035
1	Commander US Army Communications Rsch and Development Command ATTN: DRDCO-PPA-SA Fort Monmouth, NJ 07703
1	Commander US Army Electronics Research and Development Command Technical Support Activity ATTN: DELSD-L Fort Monmouth, NJ 07703
4	Commander US Army Missile Command ATTN: DRSMI-R DRSMI-YDL DRSMI-RDK Mr. R. Deep Mr. R. Becht Redstone Arsenal, AL 35809
1	Commander US Army Natick Research and Development Command ATTN: DRXRE, Dr. D. Sieling Natick, MA 01762
1	Commander US Army Tank Automotive Research & Development Cmd ATTN: DRDTA-UL Warren, MI 48090
1	Commander US Army Research Office P. O. Box 12211 Research Triangle Park NC 27709

DISTRIBUTION LIST

No. of Copies	Organization
1	Director US Army TRADOC Systems Analysis Activity ATTN: ATAA-SL, Tech Lib White Sands Missile Range NM 88002
3	Commander Naval Air Systems Command ATTN: AIR-604 Washington, DC 20360
2	Commander David W. Taylor Naval Ship Research & Development Ctr ATTN: Dr. S. de los Santos Mr. Stanley Gottlieb Bethesda, MD 20084
4	Commander Naval Surface Weapons Center ATTN: Dr. T. Clare, Code DK20 Dr. P. Daniels Mr. D. A. Jones III Mr. L. Mason Dahlgren, VA 22448
4	Commander Naval Surface Weapons Center ATTN: Code 312 Mr. S. Hastings Mr. F. Regan Mr. J. Knott Mr. R. Schlie Silver Spring, MD 20910
1	Commander Naval Weapons Center ATTN: Technical Library China Lake, CA 93555
1	AFATL/DLDL Eglin AFB, FL 32542
1	Director NASA Langley Research Center ATTN: MS-185, Tech Lib Langley Station Hampton, VA 23365
1	Director NASA Ames Research Center ATTN: MS-202, Tech Lib Moffett Field, CA 94035
1	Arnold Research Organ., Inc. von Karman Gas Dynamics Facility ATTN: Dr. John C. Adams, Jr. Aerodynamics Division Projects Branch Arnold AFS, TN 37389
1	Calspan Corporation ATTN: Mr. J. Andes, Head Transonic Tunnel Department P. O. Box 235 Buffalo, NY 14221
1	Honeywell, Inc. ATTN: Mr. George Stilley 600 Second Street, N. Hopkins, MN 55343
2	Saber Industries, Inc. ATTN: Dr. G. V. Bull Dr. D. Lister North Jay Road P. O. Box 60 North Troy, VT 05859
1	Sandia Laboratories ATTN: Div 133, H.R. Vaughn Albuquerque, NM 87115
2	Massachusetts Inst of Tech ATTN: Prof. E. Covert Prof. C. Haldeman 77 Massachusetts Avenue Cambridge, MA 02139

DISTRIBUTION LIST

No. of Copies	Organization
1	MIT/Lincoln Laboratories ATTN: Dr. Milan Vlajinac Mail Stop D-382 P. O. Box 73 Lexington, MA 02173
1	Texas A&M University College of Engineering ATTN: Dr. Robert H. Page College Station, TX 77843
1	University of Delaware Mechanical and Aerospace Engineering Department ATTN: Dr. J. E. Danberg Newark, DE 19711
1	University of Virginia Dept of Aerospace Eng and Eng Physics ATTN: Prof. I. Jacobson Charlottesville, VA 22904

No. of Copies	Organization
	Aberdeen Proving Ground
	Dir, USAMSAA ATTN: DRXSY-D DRXSY-MP, H. Cohen
	Cdr, USATECOM ATTN: DRSTE-TO-F
	Dir, Wpns Sys Concepts Team, Bldg. E3516, EA ATTN: DRDAR-ACW Mr. M. Miller Mr. A. Flatau
	Dir, CSL, Biophysics Lab, EA ATTN: Mr. W. Sacco Bldg. E3160

USER EVALUATION OF REPORT

Please take a few minutes to answer the questions below; tear out this sheet and return it to Director, US Army Ballistic Research Laboratory, ARRADCOM, ATTN: DRDAR-TSB, Aberdeen Proving Ground, Maryland 21005. Your comments will provide us with information for improving future reports.

1. BRL Report Number _____

2. Does this report satisfy a need? (Comment on purpose, related project, or other area of interest for which report will be used.)

_____

_____

_____

3. How, specifically, is the report being used? (Information source, design data or procedure, management procedure, source of ideas, etc.) _____

_____

_____

4. Has the information in this report led to any quantitative savings as far as man-hours/contract dollars saved, operating costs avoided, efficiencies achieved, etc.? If so, please elaborate.

_____

_____

5. General Comments (Indicate what you think should be changed to make this report and future reports of this type more responsive to your needs, more usable, improve readability, etc.) _____

_____

_____

_____

6. If you would like to be contacted by the personnel who prepared this report to raise specific questions or discuss the topic, please fill in the following information.

Name: _____

Telephone Number: _____

Organization Address: _____

_____

_____